

RESEARCH

Open Access



# Influence of Aeolian Sand on Capillary Water Absorption of Concrete Under Freeze–Thaw Conditions

Yugen Li<sup>1,2\*</sup> , Huimei Zhang<sup>2,3\*</sup>, Shaojie Chen<sup>2</sup>, Hairen Wang<sup>1</sup>, Xiaoyu Liu<sup>3</sup> and Wei Gao<sup>4</sup>

## Abstract

Aeolian sand (AS) can become a green resource for concrete after the reasonable utilization. Study the evolution of AS concrete (ASC) capillary water absorption (CWA) under freeze–thaw (FT) conditions is of great significance for its popularization and application. One-dimensional (1D) CWA test was performed to analyze the effects of AS and freeze–thaw cycling (FTC) on concrete water absorption characteristics. Pore relative saturation (PRS) and pore saturation were defined to reveal the influence mechanism of AS content on concrete water absorption under FT conditions and predict the moisture distribution in damaged ASC combining with the capillary mechanics theory. The results showed that concrete frost resistance increased with increased AS content and the optimal frost resistance achieved with 100% AS replacement despite its low strength. The initial water absorption rate (WAR), pore saturation, and saturation speed of the ASC decreased with increased AS, while the PRS increased with low AS content but decreased with excessive AS. The water absorption depth increased with increased mass and dynamic elastic modulus loss rates. The mechanism regarding why excessive AS improved concrete frost resistance lay in its internal pore structure and large pore ratio, which reduced pore content that can easily absorb water, enclosed a higher volume of air bubbles, and easily formed "air locking," thereby increasing water transmission resistance and forming long transmission paths during the process of CWA.

**Keywords** Aeolian sand concrete, Freeze–thaw conditions, Capillary water absorption, Moisture transmission model, Distribution prediction

## 1 Introduction

As a main component of concrete, sand is used to perfect the granular continuity between the cement and gravel. Traditionally, the sources of sand have been rivers. However, time is running out for sand (Bendixen et al., 2019). AS is widely distributed worldwide and can become a green resource for concrete after the reasonable utilization (Xue et al., 2017). Recently, researchers have studied the workability, mechanical properties, and durability of ASC from different angles, and the results shown that AS can change the interfacial transition zone (ITZ) and micro-region bleeding effect of concrete due to its physical and chemical properties, thus affecting the workability and compressive strength of concrete (Li et al., 2022; Zhang et al., 2022). Moreover, it can change the pore

Journal information: ISSN 1976-0485/eISSN2234-1315

\*Correspondence:

Yugen Li

liyugen@yulinu.edu.cn

Huimei Zhang

zhanghmktz@xust.edu.cn

<sup>1</sup> School of Architecture Engineering, Yulin University, Yulin 719000, China

<sup>2</sup> School of Architectural and Civil Engineering, Xi'an University of Science and Technology, Xi'an 710054, China

<sup>3</sup> School of Science, Xi'an University of Science and Technology, Xi'an 710054, China

<sup>4</sup> Shaanxi Shengyuan Tongtai Construction Engineering Co., Ltd, Yulin, China

structure, moisture transport path, and wet field environment of concrete, thereby altered its durability (Dong et al., 2016; Li & Shen, 2019; Li et al., 2020).

Generally, the durability of concrete is closely related to its water absorption capacity, especially in the salt lake, seasonal frozen, and salt alkali regions, which affects their working life. Previous studies have shown that the transmission of water into concrete is by CWA, supplemented by diffusion, seepage, and other processes (Bellegem et al., 2016). Moisture that enters concrete will not only lead to steel bar corrosion in reinforced concrete but also can accelerate concrete deterioration by FT conditions in cold and seasonal regions (Gonen et al., 2015). Therefore, it is of great significance to study concrete durability in terms of CWA (Zhang et al., 2018a).

CWA test was carried out according to ASTM-C1585-13 (ASTM ASC1585 2013) and Chinese Standard GB-T50082 (China Academy of Building Research, 2010) to analyze the internal moisture transmission mechanism, predict moisture distribution, and evaluate the durability of cement-based materials under salt corrosion and FT conditions. Zhang et al. (Zhang et al., 2017) have studied the effects of FT on the CWA and chloride ion permeability of concrete and found that both the CWA and chloride penetration rates increase with increasing freeze–thaw cyclings (FTCs). The reason is that the initial cracks of concrete gradually appear and develop under FTCs, which provides a channel to accelerate the moisture and chloride ion permeability. Ghasemzadeh et al. (Ghasemzadeh et al., 2016) have analyzed the water absorption capacity of damaged mortar and concluded that the initial WAR increases linearly with the damage degree in the early stage and stabilizes in the later stage. Kessler et al. (Kessler et al., 2017) have studied the effects of FT damage on chloride ingress into concrete and found that the chloride migration coefficient increases with increasing FTCs. Also, the addition of air-entraining agents effectively improves concrete frost resistance and slows chloride infiltration.

CWA of concrete is closely related to its porosity and pore structure (Zhang et al., 2018b). It is of great significance to study the effect of pore structure on CWA of concrete and predict the water distribution in it (Wang et al., 2019). Zhao et al. (Zhao et al., 2019) analyzed the relationship between pore structure and CWA capacity of cement-based materials, and found that the WAR is well correlated with the porosity and equivalent pore radius. Taniguchi and Katsura (Taniguchi & Katsura, 2015) have researched concrete water distribution using a humidity sensor, which provided a new idea for engineering practice. Bao and Wang (Bao & Wang, 2016) have analyzed the behavior of water transmission in concrete and established the moisture prediction model under continuous

axial loads. The results shown that the CWA curve presents a typical characteristic of a "bilinear" shape and the model based on unsaturated flow theory agreed well with their test results.

The results discussed above are of great significance for durability deterioration repair and the anti-deterioration design of concrete. However, most of these studies were based on the macroscopic view, there still exist some shortcomings. Currently, the influence mechanism of AS on the frost resistance of concrete needs to be further studied. In addition, there have been few reports taking into account the CWA characteristics of ASC, the prediction of moisture distribution in concrete is lacking, especially after FTC damage, which greatly restricted its popularization and application in practice.

In this study, river sand was partially replaced by AS from the desert of Northwest China to produce ASC, and its freezing resistance was studied by rapid FTC test at first. Then, the effects of AS on concrete water absorption characteristics under FT conditions were analyzed by 1D CWA test combining with the capillary mechanics theory and PRS. Finally, a water transmission model in damaged ASC was established and the distribution of moisture predicted based on pore saturation.

## 2 Materials and Methods

### 2.1 Material and Mix Ratios

Both river sand and AS were used in this experiment. River sand was medium sand, with a fineness modulus of 2.3 and apparent density of 2580 kg/m<sup>3</sup>. AS was ultrafine sand taken from the surfaces of the southern margins of the Mu Us Desert (northwest of China), with a fineness modulus of 0.9 and apparent density of 2592 kg/m<sup>3</sup>, in accordance with the Chinese Technical Code JGJ52 (JGJ 52 (2006)). The coarse aggregate was crushed limestone with a diameter range of 5–20 mm and the mass ratio of stone with diameter ranges of 5–10 and 10–20 mm was 3:7. Portland cement labeled as P·O 42.5R (Inner Mongolia Grassland brand, China) was used, with a density of 3145 kg/m<sup>3</sup>, standard water consumption of 28.6%, and the compressive strengths of 23.5 and 54.1 MPa at 3 and 28 d, respectively. Fly ash was used with the grade of II (Yushen Thermal Power Plant, China). Table 1 presents the mix proportions and materials used in this study.

### 2.2 Method

#### 2.2.1 FTC Testing

Prismatic samples 100 × 100 × 400 mm in size were used to analyze the FT damage evolution in ASC, with three pieces per sample. First, samples were cured moisturizing for 1 d, followed by curing under standard conditions of 20 ± 2 °C and 95% humidity, based on the Chinese Testing Code GB/T 50081 (GB/T 50081, 2002) for 24 d,

**Table 1** Mix ratio and the materials consumption of ASC

| Samples | Water (kg.m <sup>-3</sup> ) | Cement (kg.m <sup>-3</sup> ) | Fly ash (kg.m <sup>-3</sup> ) | River sand (kg.m <sup>-3</sup> ) | Aeolian sand (kg.m <sup>-3</sup> ) | Stone (kg.m <sup>-3</sup> ) | Air-entraining agent (kg.m <sup>-3</sup> ) | Compressive strength (MPa) |
|---------|-----------------------------|------------------------------|-------------------------------|----------------------------------|------------------------------------|-----------------------------|--|----------------------------|
| ASC0    | 190                         | 338                          | 84                            | 572                              | –                                  | 1215                        | 0.025                                      | 41.82                      |
| ASC10   | 190                         | 338                          | 84                            | 514.8                            | 57.2                               | 1215                        | 0.025                                      | 42.24                      |
| ASC20   | 190                         | 338                          | 84                            | 457.6                            | 114.4                              | 1215                        | 0.025                                      | 43.84                      |
| ASC30   | 190                         | 338                          | 84                            | 400.4                            | 171.6                              | 1215                        | 0.025                                      | 44.58                      |
| ASC40   | 190                         | 338                          | 84                            | 343.2                            | 228.8                              | 1215                        | 0.025                                      | 40.23                      |
| ASC50   | 190                         | 338                          | 84                            | 286                              | 286                                | 1215                        | 0.025                                      | 39.05                      |
| ASC100  | 190                         | 338                          | 84                            | 0                                | 572                                | 1215                        | 0.025                                      | 38.03                      |

ASC0–ASC100 represent samples with aeolian sand replacements of 0, 10, 20, 30, 40, 50, and 100%, respectively

**Table 2** Sampling times and allowable error of CWA

| Times  | 3   | 5 | 10    | 15 | 30 | 60    | 120 | 180 | 240    | 360 | 540 | 720     | 1080 | 1440 | 2520 | 2880 | 4320 | 10080 |
|--------|-----|---|-------|----|----|-------|-----|-----|--------|-----|-----|---------|------|------|------|------|------|-------|
| Errors | 5 s |   | 2 min |    |    | 5 min |     |     | 60 min |     |     | 180 min |      |      |      |      |      |       |

Sampling times represent the cumulative water absorption time of the samples (min), and “Errors” represent the error of measurement time (s or min)

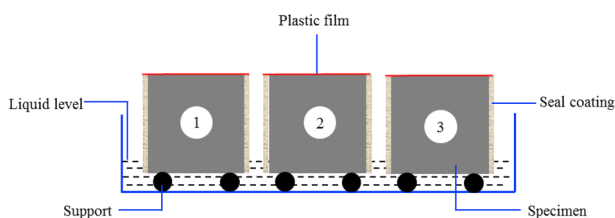


**Fig. 1** Schematic of 1D capillary absorption for concrete

and then transferred to water curing for 4 d. Finally, a KDR-V9 rapid FT testing machine was used to evaluate its frost resistance according to Chinese Standard GB/T 50082 (China Academy of Building Research, 2010), with temperatures of  $-18 \pm 2$  and  $5 \pm 2$  °C and each FTC completed within 3.5–4 h. The weight and dynamic elastic modulus of test samples were measured every 25 FTCs to track the ASC durability evolution.

### 2.2.2 CWA Testing

Cube samples 100 × 100 × 100 mm in size were used to analyze the evolution of CWA characteristics of ASC under FT conditions. After 0, 50, 100, 150, and 200 FTCs, samples were removed and dried at 105 °C for 48 h (Zhao et al., 2019). Then, the side of the pieces was sealed (Wang et al., 2019), and a 1D CWA test was performed in accordance with the conditions shown in Table 2. The mass of water absorbed by capillary action was determined by weighing; a schematic of the capillary absorption test is shown in Fig. 1.

### 2.2.3 Pore structure

Samples of  $\phi 50 \times 100$  mm were cut from 28-d cured concrete specimens to analyze the influence of AS content on the initial pore ratio and pore structure of concrete samples. First, the pieces were dried to a constant weight in an oven at 105 °C, as reported in Khatib and Clay (Khatib & Clay, 2004), and the pore ratio tested by weighing according to both the natural and vacuum saturation method for 7 d. Then, the samples were subjected to NMR analysis using a MacroMR12-150H-I instrument (NMR; Suzhou Niumag Analytical Instrument Corp., Suzhou, China) after the state of vacuum saturation to evaluate the pore size distribution.

## 3 Results and Discussion

### 3.1 Durability Deterioration of ASC under FT Conditions

When affected by FTCs, surface peeling, internal cracking, and other new damage occur in concrete samples, resulting in changes in its weight, dynamic elastic modulus, and durability degradation. Analyzing the durability evolution of concrete under FT conditions and revealing the damage mechanism are of great importance for engineering practice.

Generally, the mass loss rate and dynamic elastic modulus loss rate as shown in Eqs. 1 and 2 were used as damage variables to evaluate the frost resistance of concrete (Xiao et al., 2019a, 2019b). Fig. 2 shows the evolution of these 2 indicators of ASC under FT conditions taking ASC0, ASC30, ASC50, and ASC100 as examples.

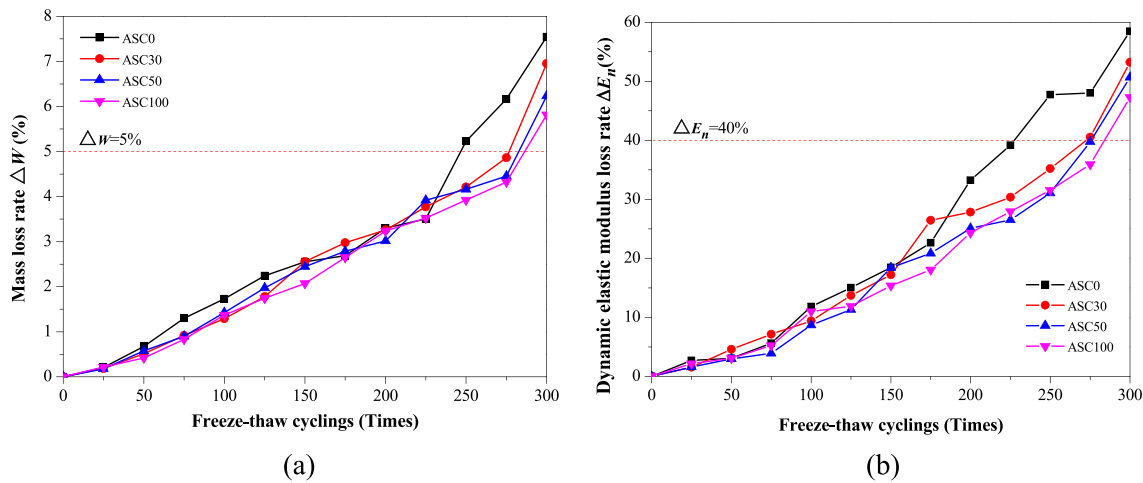


**Fig. 2** Relationships among mass loss rate, dynamic elastic modulus loss rate, and FTCs **a** Mass loss rate, **b** Dynamic elastic modulus loss rate

$$\Delta W = \frac{W_0 - W_n}{W_0} \times 100\%, \tag{1}$$

$$\Delta E_n = \frac{E_0 - E_n}{E_0} \times 100\% \tag{2}$$

where  $\Delta W$  and  $\Delta E_n$  are the mass loss rate and dynamic elastic modulus loss rate, respectively;  $W_0$  and  $E_0$  are the initial mass and initial dynamic elastic modulus, respectively;  $W_n$  and  $E_n$  are the mass and dynamic elastic modulus of concrete after  $n$  FTCs, respectively.

As can be seen in Fig. 2, both the loss rate of mass and dynamic elastic modulus of ASC increased nonlinearly with the increasing FTCs, with the rate slow at first and then becoming fast. Specifically, there was little difference in mass loss rate and dynamic elastic modulus loss rate of each sample in the initial FT stage, and then the difference gradually increased.

With the dynamic elastic modulus loss rate at 40% or the mass loss rate at 5% as the failure criterion according to Chinese Standard GB/T 50082 (China Academy of Building Research, 2010), ASC0 was considered destroyed after 225 FTCs. ASC30 and ASC50 samples were observed to lose their frost resistance after 275 cycles, and ASC100 damaged after 300 cycles. After 300 FTCs, the mass loss rates of ASC0, ASC30, ASC50, and ASC100 samples were 7.55, 6.95, 6.23, and 5.82% and the dynamic elastic modulus loss rates at 58.49, 53.22, 50.67, and 47.28%, respectively. That is, the ASC damage degree caused by FT roughly decreased with

increased AS content, which was different from the relationship between the initial concrete strength at 28 d and AS content (Table 1). The reasons for these results were analyzed below.

### 3.2 Evolution of ASC Water Absorption under FT Conditions

#### 3.2.1 Cumulative Water Content

The CWA process of porous materials, such as concrete, can be described by Darcy’s Law and its absorption water capacity can be characterized by the CWA rate “ $S$ ” or cumulative water content “ $I$ ” per unit area. The relationship between  $S$  and  $i$  is (Hall, 1989; Martys & Ferraris, 1997)

$$i = S\sqrt{t} + b \tag{3}$$

where  $t$  is water absorption time (s),  $b$  is the intercept on the vertical axis, and  $S$  is the initial WAR, which can be obtained by linear fitting of the first 6-h data of  $i-\sqrt{t}$  curve (ASTM C1585-13, 2013). For damaged concrete,  $S$  reflected the internal damage degree to a certain extent, such that the larger the value was, the more serious the concrete damage, the stronger the water absorption capacity, and the worse the frost resistance.

The cumulative water content  $i$  was calculated according to Eq. 4, as

$$i = \frac{m_t}{a \cdot d} \tag{4}$$

(See figure on next page.)

**Fig. 3** Curves of cumulative water content per unit area with square root of time **a** ASC0 (0–7 d), **b** ASC0 (0–6 h), **c** ASC30 (0–7 d), **d** ASC30 (0–6 h), **e** ASC50 (0–7 d), **f** ASC50 (0–6 h), **g** ASC100 (0–7 d), **h** ASC100 (0–6 h)

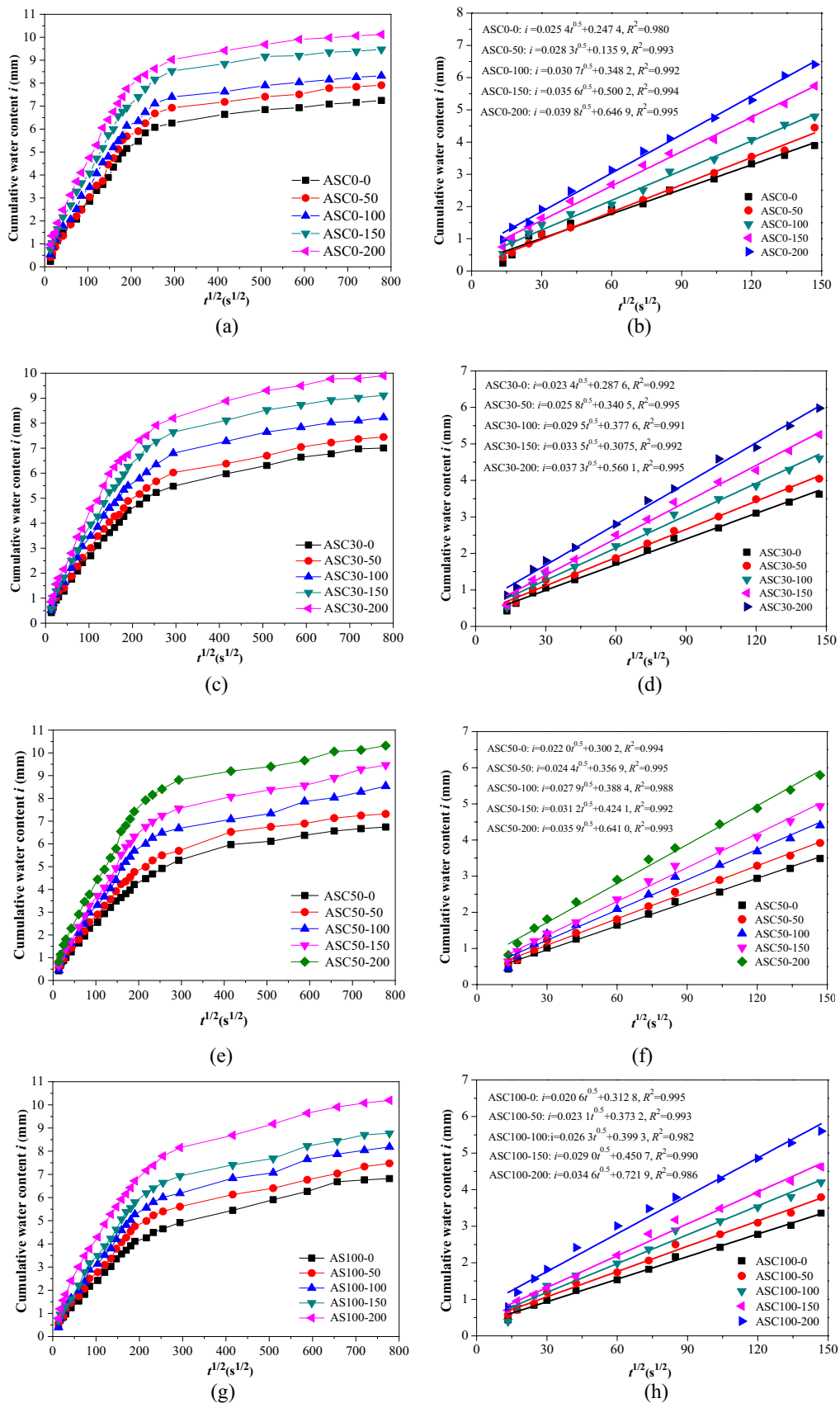
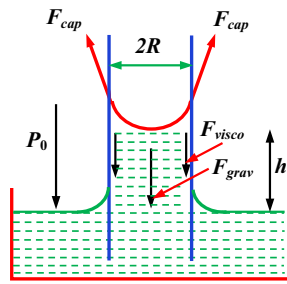


Fig. 3 (See legend on previous page.)



**Fig. 4** Schematic diagram of liquid force in capillary

where  $m_t$  is the sample water absorption weight at time  $t$  (g),  $a$  is the water absorption area ( $\text{mm}^2$ ), and  $d$  is the water density ( $\text{g}/\text{mm}^3$ ). Fig. 3 shows the relationship between the cumulative water content  $i$  and square root of time of ASC under FT conditions.

It was easily observed that the water absorption process of ASC under FT conditions was similar to that of ordinary concrete (ASC0). Both aspects experienced a trend of first a rapid increase, followed by slowing and final stabilization, and the water absorption curve showed a typical characteristic of being “bilinear.” Meanwhile, the cumulative water content of each sample increased with increased FTCs.

The main reason why the water absorption speed showed a tendency to start fast and then slow was due to the complicated process of liquid capillary flow, which has different rising mechanisms in different water absorption periods. According to capillary mechanics theory, liquid in a capillary tube is mainly affected by the capillary pressure  $F_{cap}$ , tube wall viscous resistance  $F_{visco}$ , and gravity  $F_{grav}$  (Fig. 4). These factors determine whether moisture can be absorbed into the concrete as the result of their common action. At the beginning, less moisture was absorbed into the concrete, such that  $F_{visco}$  and  $F_{grav}$  were ignored. At this time, water was quickly absorbed into the concrete under the action of  $F_{cap}$ , with the smaller the pore radius, the faster the water absorption speed and higher the liquid rising. Later, the moisture absorbed into the concrete gradually increased and the obstructive effect of  $F_{visco}$  and  $F_{grav}$  on the liquid increased, resulting in a weakening of the water absorption power and a slower rate.

In addition, the water absorption speed was significantly affected by the humidity gradient in and outside of the concrete as well as the pore structure. The larger the gradient, the more water easily absorbed into water capillaries and the faster the water absorption speed. With increased water absorption time, the humidity gradient in and outside the concrete gradually decreased, such that the moisture transmission path

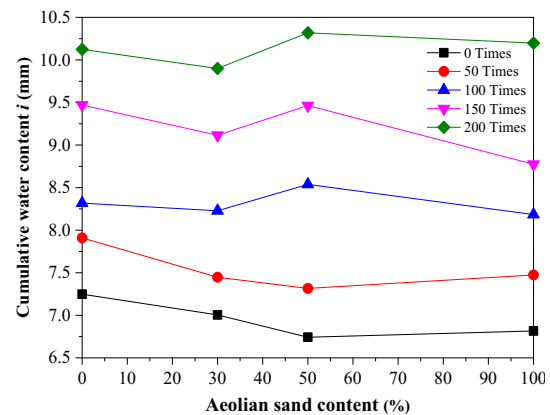


**Fig. 5** Relationship between final cumulative water content and AS content

became longer, which also slowed the water absorption speed.

Notably, the relation between the final cumulative water content and AS amount exhibited a different trend at different FT stages (Fig. 5). When the FTCs were  $<100$ , the final water absorption content first showed a decrease and then increased with increased AS. Later, the relationship shows an “S” shape, which was not completely consistent with the concrete damage degree and the initial pore ratio. The reason for this observation was attributed to two aspects. On one hand, the air bubble enclosed in concrete during the production process affects the pore saturation speed and the CWA capacity of ASC under different FT stages, thereby might have affected the final water absorption capacity of samples. On the other hand, the internal pore ratio, pore structure, and gradient of the wet field change during the FT process, which might have also affected the speed and path of water absorption, as well as the final cumulative water content.

Taking into account the short water absorption time of concrete in the thawing stage, the initial WAR was used to approximate the evolution of ASC water absorption characteristics under FT conditions. Linear regression analysis showed that the relationship between the cumulative water content  $i$  and the square root of time  $\sqrt{t}$  of each sample agreed well with Eq. 3 at the initial stage, with a correlation coefficient of  $R^2 \geq 0.98$  (Figs. 3b, d, f, and h).

For intuitiveness, Fig. 6 shows the relationships between the initial WAR  $S_1$ , increased FTCs and AS content. As can be seen that  $S_1$  gradually increased with increased FTCs (Fig. 6a). The reason was that the FT action affected the concrete pore ratio (Fig. 7), thus increasing the pore content that was prone to CWA and making it easier for water to enter the concrete, thus

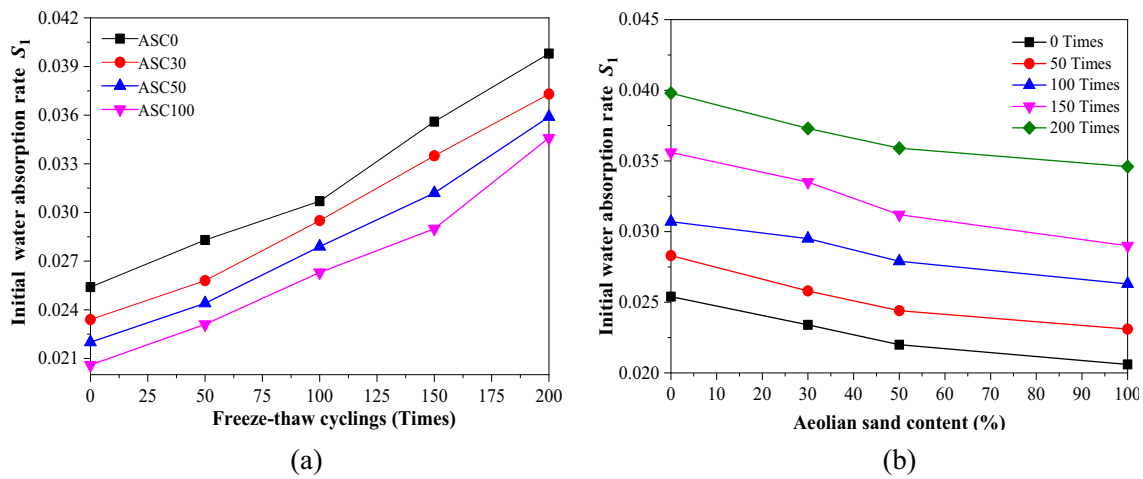


**Fig. 6** Relationship between concrete initial absorption rate and FTCs. **a**  $S_1$  and FTCs. **b**  $S_1$  and AS content

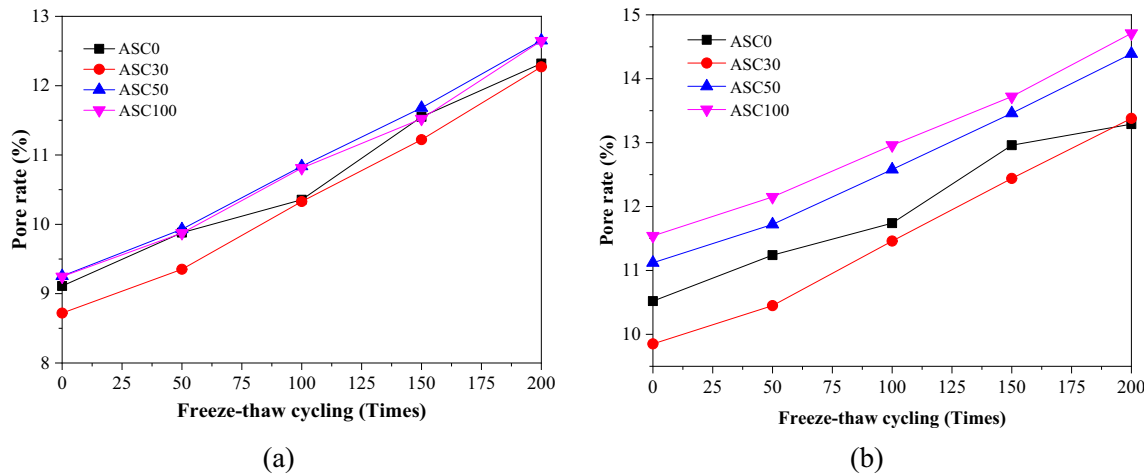


**Fig. 7** Evolution curves of pore density under FT conditions. **a** Natural saturation. **b** Vacuum saturation

increasing the initial WAR. Meanwhile,  $S_1$  decreased with increased AS under the given FTC (Fig. 6b) and the reasons are analyzed below.

### 3.2.2 Pore Saturation

The concrete damage caused by FT is closely related to its internal pore saturation rate and saturation (Gerdes et al., 1998; Tan et al., 2017). The evolution of ASC pore saturation rate and saturation with the length of water absorption time under FT conditions were analyzed. The pore saturation  $S_{aq}$  in concrete was defined as

$$S_{aq} = \frac{V_t}{V} \times 100\%, \tag{5}$$

where  $V_t$  is the volume of water in concrete pores corresponding to the water absorption time  $t$  ( $\text{cm}^3$ ) and  $V$  is the pore volume in concrete measured after a CWA time of 7 d (considered saturated,  $\text{cm}^3$ ).

For water, when its density was  $1 \text{ g/cm}^3$ , the weight of absorbed water at time  $t$  was equal in quantity to the volume, such that Eq. 5 was expressed as

$$S_{aq} = \frac{m_t}{m_{aq}} \times 100\%, \tag{6}$$

where  $m_t$  and  $m_{aq}$  are the cumulative water absorption weight of concrete at time  $t$  and the saturation state, respectively (g).

According to Eq. 6, the relationship between  $S_{aq}$  and  $\sqrt{t}$  of ASC after different FTCs was obtained. It was not difficult to see that the water absorption saturation

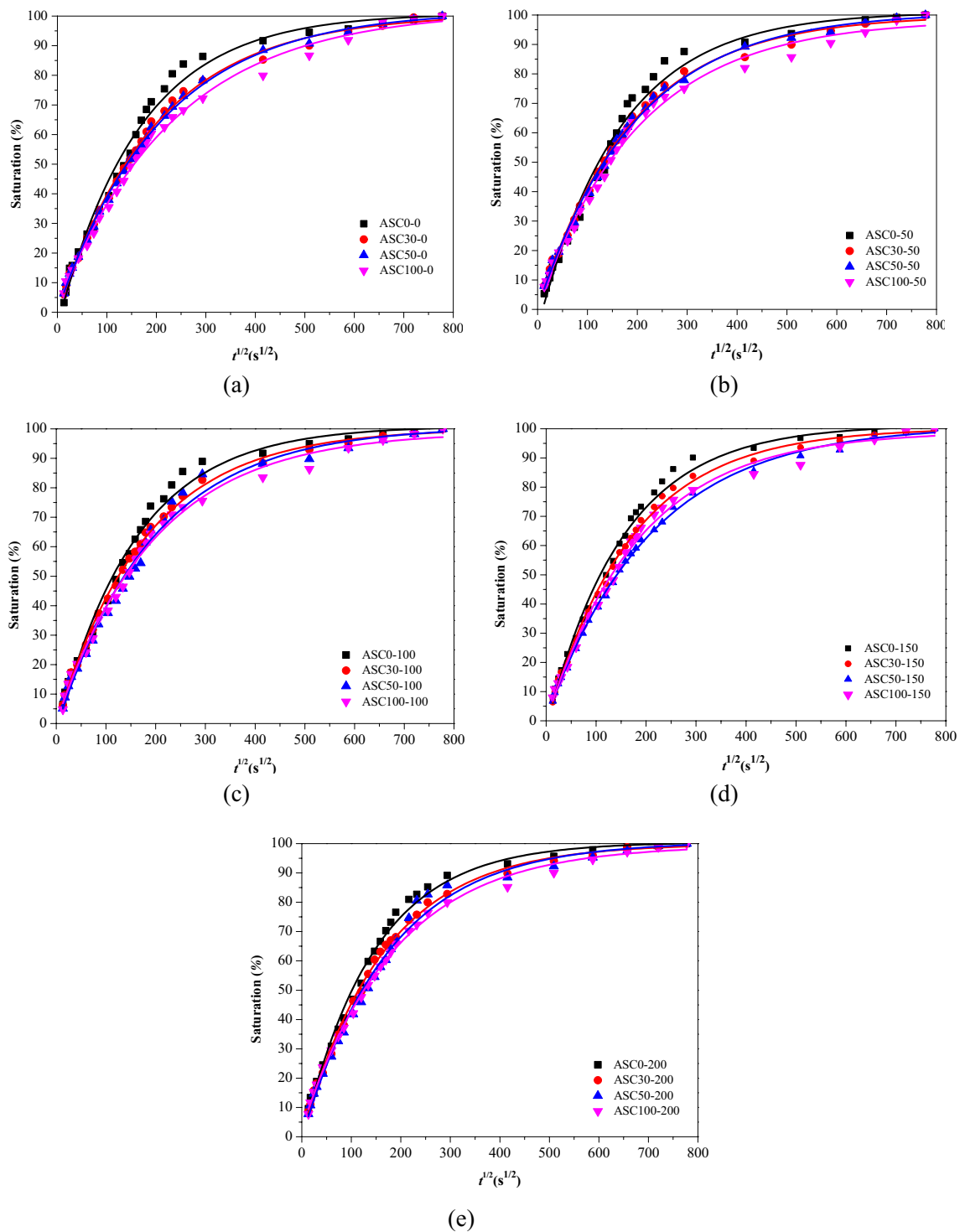


**Fig. 8** Relationship between pore saturation and square root of time of ASC. **a** 0 Times, **b** 50 Times, **c** 100 Times, **d** 150 Times and **e** 200 Times

of pores in ASC increased nonlinearly with increased time, first rapidly and then slowly (Fig. 8). Overall, the pore saturations of the samples showed a general order of  $ASC0 > ASC30 > ASC50 > ASC100$  after the same

exposure time and the fixed FTC, but the difference between ASC30 and ASC50 was small in their early stages.

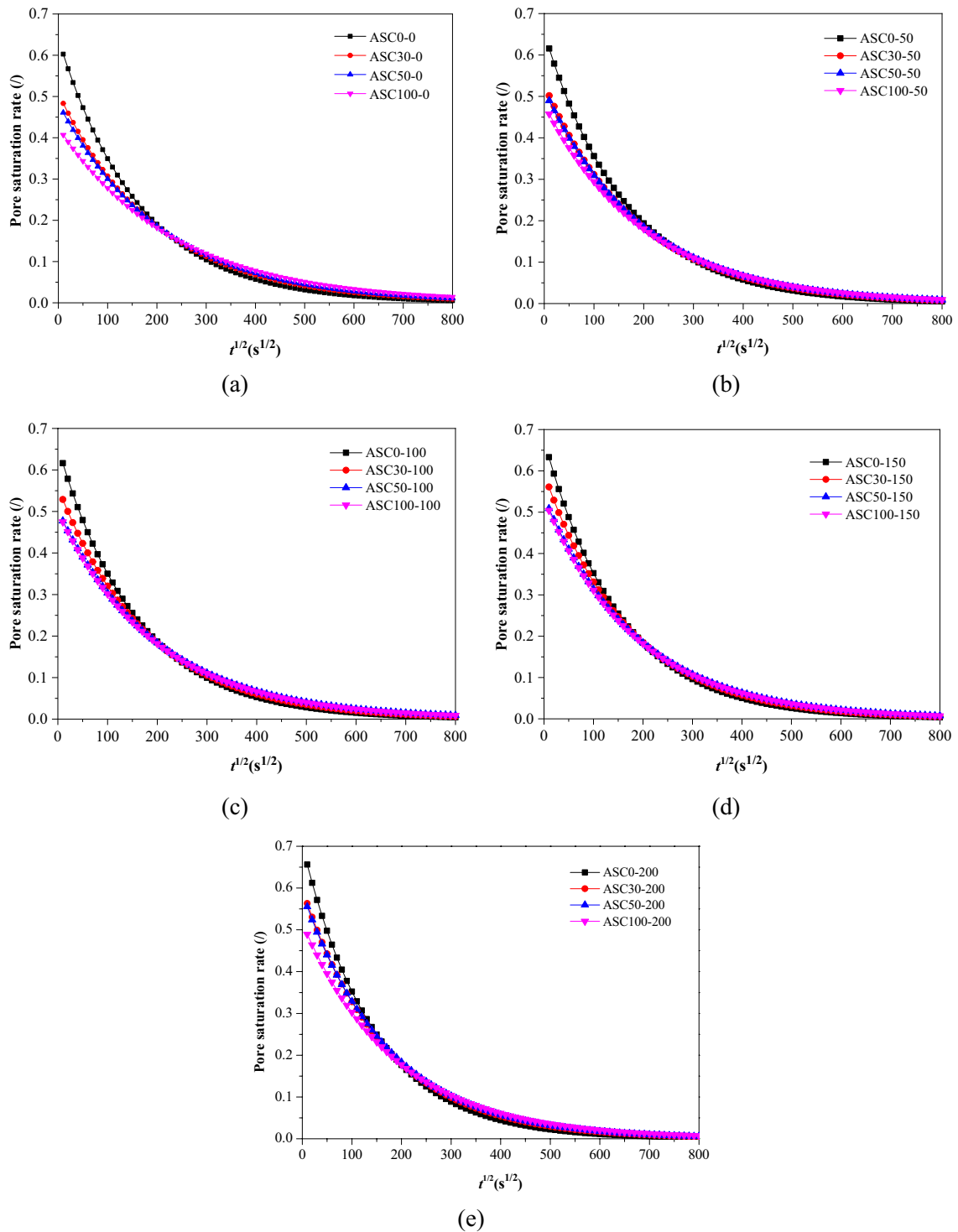


**Fig. 9** Relationship between pore saturation rate, AS content, and FTCs. **a** 0 Times, **b** 50 Times, **c** 100 Times, **d** 150 Times, and **e** 200 Times

Further analysis showed that there was an exponential function between the pore saturation of ASC and the square root of time (Eq. 7) with the correlation coefficient of  $R^2 \geq 0.98$ , and the regression curves are shown in Fig. 8.

$$S_{aq} = A + Be^{-\sqrt{t}/C}, \tag{7}$$

where  $A$ ,  $B$ , and  $C$  are the test coefficients related to the concrete mix ratio and  $t$  is the cumulative time of water absorption (s).

Taking the derivative of Eq. 6 and combining it with the water absorption data (Fig. 8), the evolution of ASC pore saturation velocity with the square root of time under FT conditions was obtained (Fig. 9).

It was easy to see that the pore saturation velocity decreased nonlinearly with increased square root of time with the rate rapid at first, then slowing, and finally stabilizing. The pore saturation rate increased with increased FTCs when AS content was fixed. The reason for these results was that frost heave stress generated by the phase transition of water to ice at low temperature during the freezing process compressed the pore walls, which resulted in an effect of hole expansion with thawing. When the stress exceeded the ultimate material strength, cracks and other new damage formed around pore walls, with damage continuing to extend into the matrix. This allowed closed and disconnected pores in concrete to gradually connect to provide more channels for CWA. As a result, the dissolution and compression speed of air bubbles in the pores were accelerated, thus speeding up the pore saturation rate.

Notably, the pore saturation velocity exhibited different trends with increased AS content when the

time was fixed. At the initial stage, the relationship of pore saturation velocity to AS of each sample was  $ASC0 > ASC30 > ASC50 > ASC100$ , which agreed well with the degree of FT damage. This roughly evolved to  $ASC100 > ASC50 > ASC30 > ASC0$  at the middle and late stages, but there were little differences among all samples, which have been caused by variation in air bubble volume in samples due to AS presence.

### 3.3 Effect Mechanism of AS on Frost Resistance and Water Absorption of Concrete

AS affected the frost resistance and water absorption of concrete, such that, in general, FT fatigue life increased with increased content (Figs. 2 and 3). However, the final cumulative water absorption content and pore saturation speed showed different tendencies with increased AS. The influencing mechanism was summarized below.

#### 3.3.1 Changing of the Pore Ratio and Pore Structure

Concrete is a typical porous material that contains gel holes, capillary holes, and other initial defects during the forming stage. AS addition can change the internal pore ratio and pore structure of concrete due to its particle gradation, surface morphology, and water absorption capability (Fig. 10). The pore rate of ASC was observed to first decrease and then increase as the AS dosage increased. The reason for this was that a proper amount of AS was perfect in the particle gradation of the concrete materials, allowing the cement particles, fly ash, AS, river sand, and coarse aggregates form a continuous gradation accumulation system, thus reducing the pore ratio and pore diameter due to AS's small particle size and round surface, which thereby improved frost resistance.

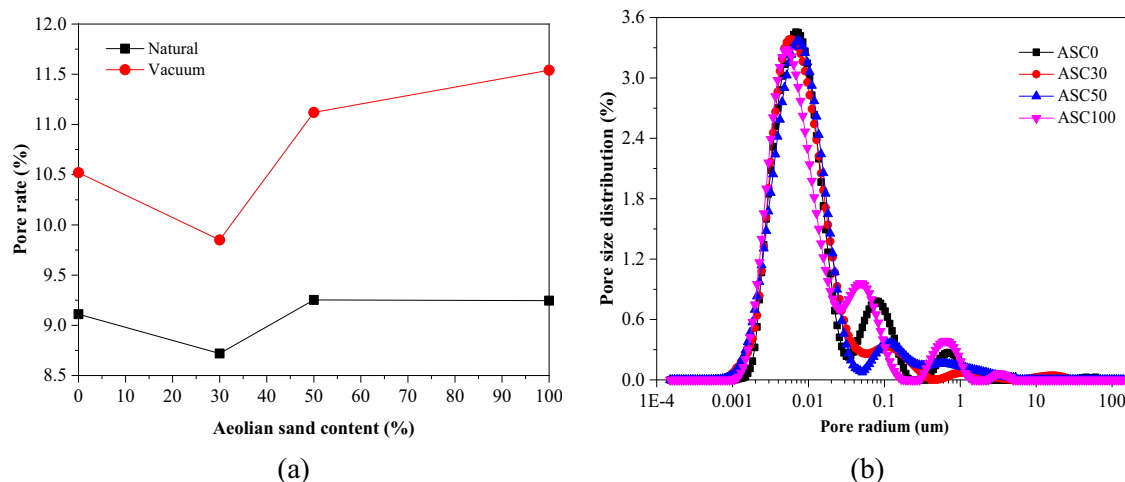
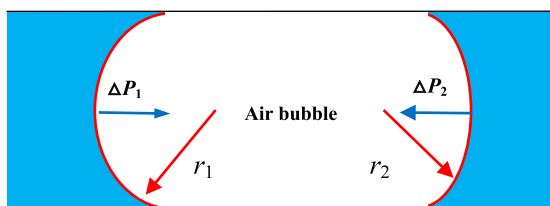


Fig. 10 Pore ratio and pore structure of ASC. a Pore ratio and b Pore structure



**Fig. 11** “Air locking” phenomenon during CWA

However, particles with poor gradation or similar size can form larger voids than well-graded particles when used to produce concrete because of the more likely occurrence of the “arch bridge” effect among particles, which is easily to settle during the process of vibrating. An excessive amount of AS resulted in a deletion of gradation, particularly for particles >0.315 mm in diameter. As a result, this increased the pore ratio and decreased the content of pores that easily absorbed water, resulting in changes in concrete frost resistance and water absorption capacity.

**3.3.2 Changing of the Pore Saturation Speed**

Water absorption saturation speed of concrete is closely related to the pore structure and air bubble content. A certain volume of air bubbles is enclosed in concrete during the production process, which also affects the pore saturation speed. When the moisture migrates to the inside of pores as capillary adsorption, a concave liquid surface forms at the air bubble of pores or cracks. “Air locking” occurs due to this surface tension and the differences liquid surface curvature between the inner and outer surfaces of the bubble (Fig. 11). As a result, the bubble dissolution time is longer, the CWA slows, and some pores are difficult to fill with water. The larger the bubble volume is, the more complex the concrete internal pore structure, the more obvious the “air locking,” the longer the time for compression or dissolution of the air bubble, and the more beneficial the resulting frost resistance of the material. This is the reason why the addition of an air-entrainment agent in engineering practice improves concrete frost resistance.

Samples with higher proportions of AS contained more air bubbles than other samples during preparation due to poor particle gradation, which was more likely to form “air locking” and made it more difficult to reach the saturation state under natural saturation conditions, which would normally improve concrete frost resistance. The PRS was used to further confirm this conjecture as shown in Eq. 8:

$$S_r = \frac{\phi_N}{\phi_V} \times 100\% \tag{8}$$

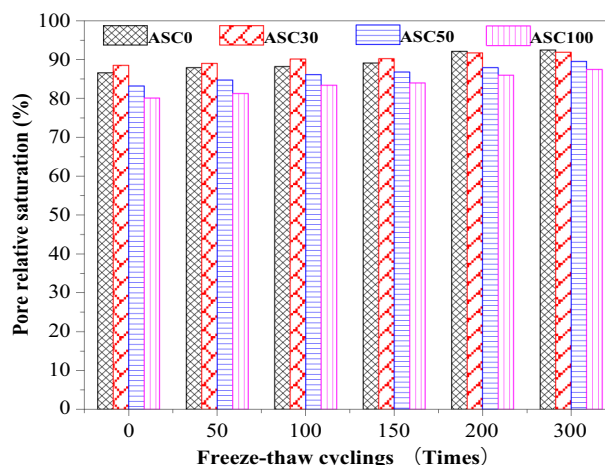


**Fig. 12** Pore relative saturation under FT conditions

where  $\Phi_N$  and  $\Phi_V$  are the natural and vacuum saturation pore ratio of concrete, respectively.

The PRS was observed to increase with increased FTCs under a given AS content (Fig. 12). While PRS first increased and then decreased before 150 FTCs, it then decreased with increased AS when the FTCs were fixed. This better revealed the mechanism by which concrete frost resistance was improved with increased AS, except for ASC30 samples at the initial and middle stages of FT. The main reason why ASC30 possessed a higher PRS than that of ASC0, but had mild freeze damage before 150 FTCs, was that a proper AS amount perfected the pore structure. This increased the content of pores that were prone to CWA in the sample, thus allowing it to reach a saturation state more easily. However, a portion of the moisture stored in these small pores did not completely freeze under low temperature conditions in this study, thus reducing the damage (Li et al., 2022).

**3.3.3 Changing of the Effective Water–Cement Ratio of Concrete**

The water–cement ratio also affects the water absorption capacity and frost resistance of concrete. The lower the water–cement ratio is, the lower the water absorption capacity of cement paste and the better the concrete frost resistance (Liu et al., 2021). Compared with river sand, AS has a stronger water absorbing capacity based on its large specific surface area, which can reduce the effective water–cement ratio of concrete to a certain extent when used to produce concrete with a fixed water–cement ratio. As a result, the initial WAR and pore saturation speed of concrete decreased with increased AS, thereby improving frost resistance.

### 4 Prediction of Moisture Distribution under FT Conditions

#### 4.1 Establishment of the Model

The present results described above showed that the CWA rate of damaged concrete increased with increased FTCs. That is, the moisture inside the concrete increased gradually with increased FT effects when the water absorption time was fixed. This is the fundamental reason for aggravated damage in concrete caused by FT. Therefore, it was necessary to analyze the transmission of moisture in damaged concrete. Assuming that the moisture only entered the interior of concrete through CWA (regardless of gravity and seepage) and that the process of moisture transmission under the action of 1D CWA can be described by Eq. 9 (Wang, 2009),

$$\frac{\partial \Theta}{\partial t} = \frac{\partial}{\partial x} \left( D(\Theta) \frac{\partial \Theta}{\partial x} \right), \tag{9}$$

where  $D(\Theta)$  is the hydraulic diffusion coefficient based on the volumetric water content  $\Theta$  and  $x(t)$  is the water absorption depth corresponding to time  $t$ .

Introducing the relative water content  $\theta$  (Eq. 10), the 1D CWA transmission equation, expressed using  $\theta$ , was expressed as Eq. 11:

$$\theta = \frac{\Theta_t - \Theta_0}{\Theta_s - \Theta_0}, \tag{10}$$

$$\frac{\partial \theta}{\partial t} = \frac{\partial}{\partial x} \left( D(\theta) \frac{\partial \theta}{\partial x} \right), \tag{11}$$

where  $D(\theta)$  is the hydraulic diffusion coefficient based on the relative water content  $\theta$ , which was expressed in the form of exponential or power function;  $\Theta_t$  is the volumetric water content in concrete at time  $t$ , which was determined using the saturation equation (Eq. 7); the pore ratio  $\rho$  is measured by the natural saturation method; and  $\Theta_0$  and  $\Theta_s$  are the initial and final water content, respectively.

When the concrete absorbing water in the state of naturally absolutely dry, there existed a boundary condition of “ $\Theta_0 \approx 0, \Theta_s \approx \rho$ ” (Hall, 1989). Thus, Eq. 10 was approximated and written as

$$\theta = \frac{\Theta_t}{\rho} = \left( A + B e^{-\frac{\sqrt{t}}{C}} \right). \tag{12}$$

It was not difficult to find that the relative water content  $\theta$  in concrete at time  $t$  (Eq. 10) was actually the pore saturation  $S_{aq}$ . Substituting  $\theta$  into Eq. 11, the CWA equation was expressed by  $\theta$ . Considering that it was a nonlinear function, the Boltzmann variable is usually introduced to find its approximate solution. Based on this, Parlange et al.

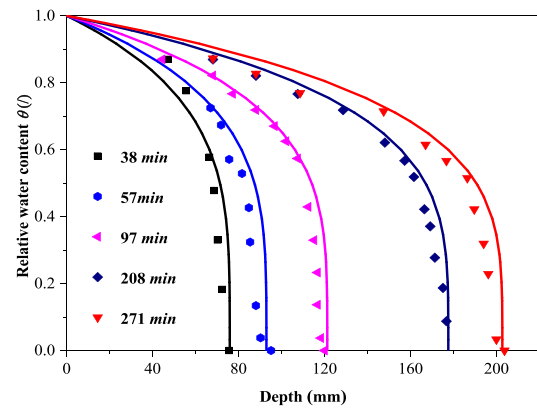


Fig. 13 Verification results of moisture transport model

(Parlange et al., 1984) have provided the approximate solution with high precision in Eq. 13, expressed as

$$x(t) = \phi \sqrt{t} = \frac{-s + \sqrt{s^2 + 4A\lambda(\theta)}}{A} \sqrt{t}, \tag{13}$$

where  $s$  is the relative WAR, calculated using Eq. 14;  $\phi$  is the Boltzmann variable;  $A$  and  $\lambda(\theta)$  are the test coefficients (model parameters), calculated by Eqs. 15 and 16, expressed as

$$s = \frac{S}{\Theta_s - \Theta_0} \approx \left( \int_0^1 (1 + \theta) D(\theta) d\theta \right)^{0.5}, \tag{14}$$

$$A = 2 - \frac{s^2}{\int_0^1 D(\theta) d\theta}, \tag{15}$$

$$\lambda(\theta) = \int_{\theta}^1 \frac{D(\theta)}{\theta} d\theta \tag{16}$$

The hydraulic diffusion coefficient  $D(\theta)$  was written as Eq. 17 when expressed by the power function (Lockington et al., 1999), as

$$D(\theta) = D_0 \theta^n, \tag{17}$$

where  $D_0$  is the empirically fitted constants, calculated by Eq. 18:

$$D_0 = \frac{(1+n)(2+n)s^2}{3+2n}. \tag{18}$$

Substituting Eq. 17 into Eqs. 15 and 16,  $A$  and  $\lambda(\theta)$  were expressed as

$$A = \frac{1}{2(2+n)}, \tag{19}$$

$$\lambda(\theta) = \frac{D_0}{n} (1 - \theta^n). \tag{20}$$

The range of parameter  $n$  in Eq. 17 is generally 4–6 and the lower limit of 4 usually used. When  $n=4$ , it was obtained that.

$$D_0 = \frac{30s^2}{11}, A = \frac{1}{12}, \lambda(\theta) = \frac{30s^2}{44} (1 - \theta^4).$$

Substituting  $A$  and  $\lambda(\theta)$  into Eq. 13 finally the moisture transmission model of ASC under FT conditions was obtained as shown in Eq. 21.

$$x(t) = 12s \left( \sqrt{1 + \frac{5}{22} (1 - \theta^4)} - 1 \right) \sqrt{t} \tag{21}$$

### 4.2 Verification of the Model

The distribution of water in mortar in a previous study (Hall, 1989) was used to verify the present established model (Fig. 13). The used mortar samples were  $235 \times 33 \times 33$  mm, the mix ratio of cement:lime:sand at

1:3:12 (by wt), pore density at 0.27, WAR at 2.57 mm/min<sup>0.5</sup>, and water–cement ratio at 4.5. The water absorption depth was seen to be predicted by Eq. 21, which agreed well with the depth obtained by the NMR imaging analysis, which indicated that the moisture transmission model established in damaged concrete according to pore saturation was reliable.

### 4.3 Distribution of Moisture in ASC under FT Conditions

Combining the CWA test results and Eq. 21, the moisture distributions in ASC damaged by FT after different water absorption times were predicted. The variation of water absorption depth with FTCs, taking 100 min as an example, is shown in Fig. 14.

It was observed that the larger the number of FTCs was, the greater the depth of water absorption when the concrete mix ratio was fixed. Specifically, the depth of each sample varied greatly after different FTCs when  $\theta$  (pore saturation  $S_{aq}$ ) was small, while it gradually decreased as  $\theta$  increased. The reason for this was the

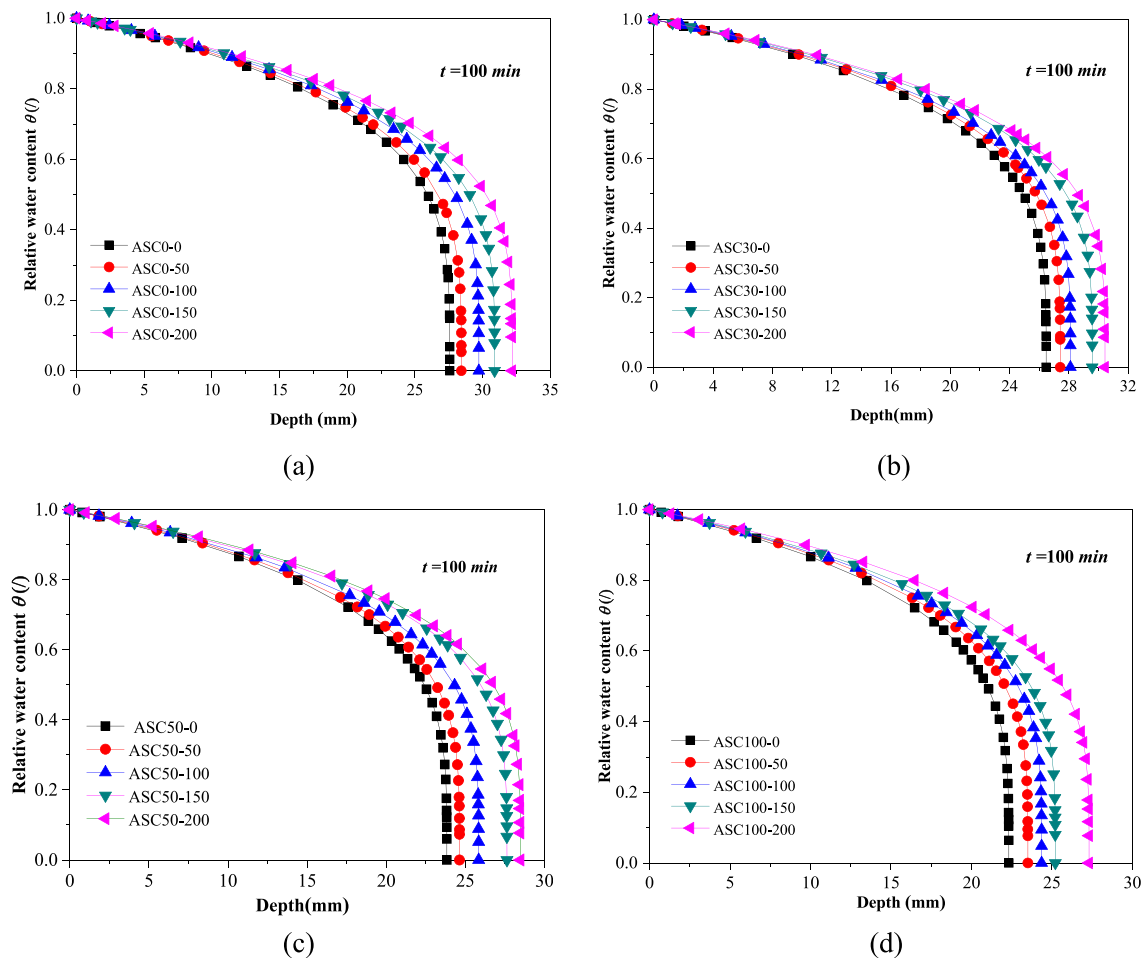


**Fig. 14** Relationship between water absorption depth and FTCs of ASC. **a** ASC0, **b** ASC30, **c** ASC50, and **d** ASC100

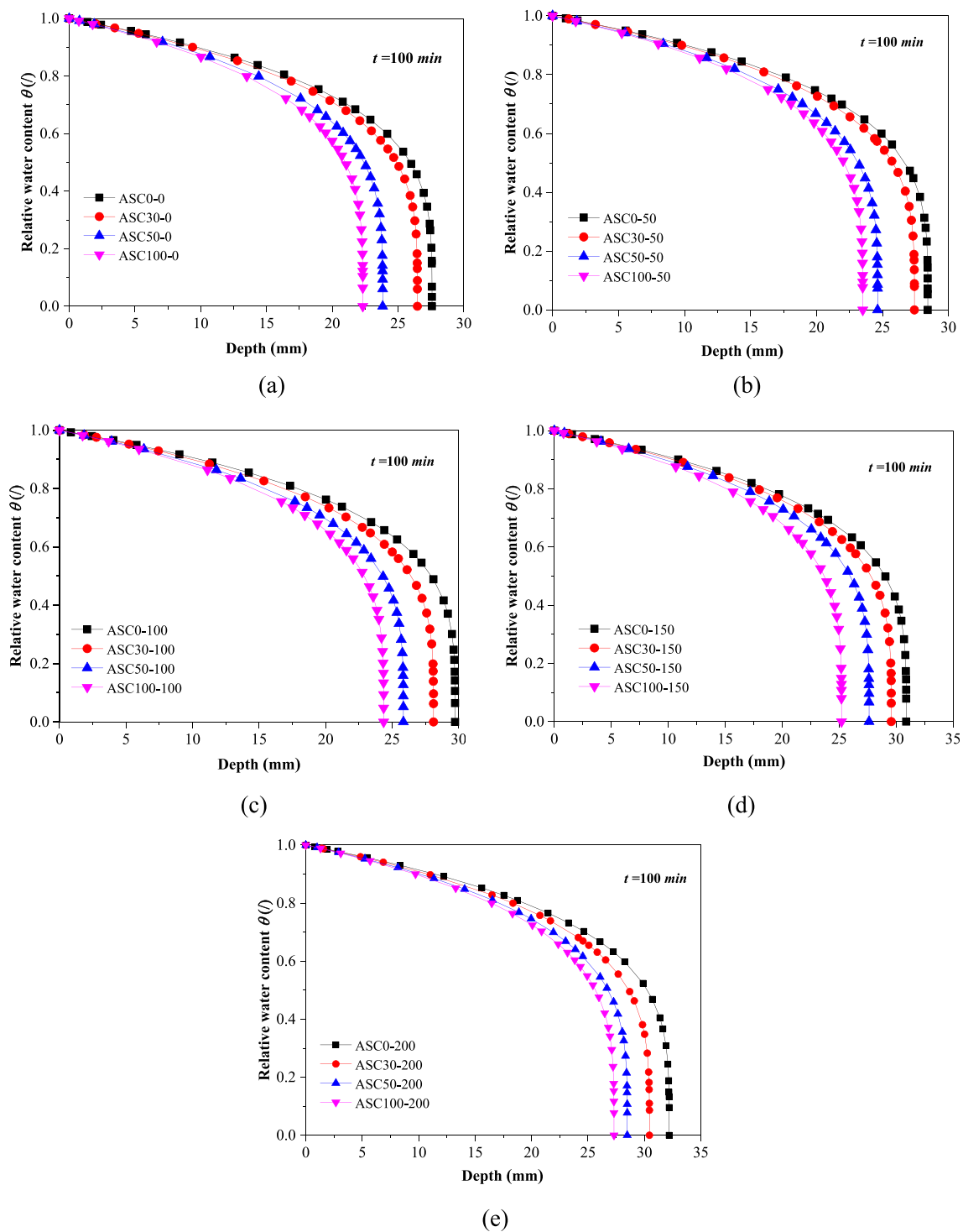


**Fig. 15** Relationship between water absorption depth and AS content of ASC. **a** 0 Times, **b** 50 Times, **c** 100 Times, **d** 150 Times, and **e** 200 Times

effect of FT changes on the internal structure and pore density of ASC, thereby increasing the depth of water absorption.

Examining the relationship between water absorption depth and AS content, the water absorption depth of each sample was seen to be different after the same number

of FTCs (Fig. 15). An approximate order of the water absorption depth was  $ASC0 > ASC30 > ASC50 > ASC100$  when the FTC number was fixed, that is, the depth decreased with increased AS. The trend of water absorption depth changes related to AS content and the number of FTCs were consistent with the loss degree of the concrete macro-freezing resistance index (mass and dynamic elastic modulus).

Quantitative analysis showed that the water absorption depth of ASC0 samples evolved from 27.58 mm in the undamaged state to 32.19 mm after 200 FTCs, increasing by 16.72%. Correspondingly, ASC30 samples evolved from 26.47 to 30.44 mm with an increment of 14.99%, while ASC50 samples evolved from 23.83 to 28.48 mm with an increment of 19.51% and ASC100 samples evolved from 22.32 to 27.31 mm with an increment of 22.36%. This also indicated that there existed little difference in water absorption depth of ASC before and after the effects of FT, even for ASC100 samples, with an increase of only 22.36%.

The reason for differences in the water absorption depth in concrete samples before and after FTCs was due to their different internal pore structure and pore ratio. For undamaged concrete, the interior, especially the floating slurry near the surface, contained a large number of capillary-size pores. When it came into contact with water, moisture quickly entered the concrete interior through these pores until it was saturated, making the surface layer much more saturated than the interior. After entering the freezing stage, the temperature of depth regions were high inside and low outside, causing water in the surface layer to freeze first and expand in volume, resulting in freezing damage. This was why

concrete deterioration caused by FTCs always started with spalling damage.

According to the Gibbs–Thomson theory (Liu et al., 2014), the larger the porosity and pore size are, the greater the saturation, the lower the freezing temperature, and the more severe the FT damage. With the progressive effects of FTCs, the original pores and cracks in the concrete continue to develop and expand, with new damage occurring. This reduced the content of pores that are prone to have capillary phenomenon and weakened the speed of water absorption. At this time, moisture mostly entered the concrete through the combined effects of capillary and seepage, resulting in the increasing pore saturation in the concrete, especially when the material was completely immersed in the water environment.

#### 4.4 Relation Between the Damage and Water Absorption Depth of ASC

The depth of water absorption was observed to be closely related to the concrete damage degree under FT conditions. Samples of ASC0, ASC30, ASC50, and ASC100 were used to analyze the evolution of water absorption depth in relation to the mass loss and dynamic elastic modulus loss rates (Fig. 16). As can be seen that the water absorption depth increased with both increased mass loss and dynamic elastic modulus loss rates. The main reason for this was that absorbed water underwent a phase change under low temperature conditions, resulting in volume expansion and the development of freeze stress, which damaged the pores and the mortar matrix near the ITZ, thereby provided new channels for CWA. The more serious the damage, the faster the saturation

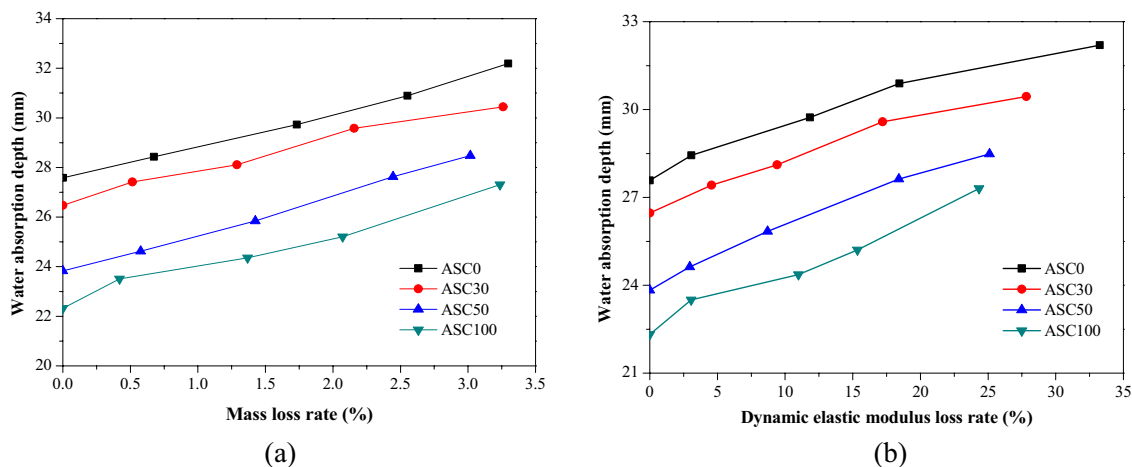


**Fig. 16** Relationships among the water absorption depth and damage variables of ASC. **a** Mass loss rate and **b** Dynamic elastic modulus loss rate

rate, the greater the water absorption depth was. The present results indicated that the depth of water migration had an important influence on the damage degree of concrete under FT conditions.

## 5 Conclusions

In this study, the evolution of durability deterioration and water absorption characteristics of ASC under FT conditions were examined. The results revealed the influence mechanism of AS on frost resistance and CWA of concrete. A moisture transmission model in damaged concrete was established, the moisture distribution depth predicted, and the relation between the water absorption depth and concrete damage degree analyzed. The conclusions were as follows:

- (1) AS affected concrete frost resistance, such that the higher the AS content was, the better the frost resistance. The best frost resistance was achieved with 100% AS content, which was 19.49% higher than that of ordinary concrete (ASC0).
- (2) The CWA curves of ASC under FT conditions presented a typical "bilinear" form with the square root of water absorption time. The initial WAR and pore saturation rate both decreased with increased AS content and increased with increased FTCs.
- (3) The water transmission model based on the pore saturation can forecast water distribution better. Water absorption depth increased with increased FTCs and decreased with increased AS.
- (4) The influence mechanism of AS on the frost resistance and CWA of concrete was that it changed the concrete's initial porosity and pore structure, which affected the air bubble content and PRS in it, thereby slow down the moisture transmission speed and reduce freezing damage.

## Acknowledgements

The authors appreciate the financial supports from the National Natural Science Foundation of China (Nos. 52268047, 51868075), Ministry of Housing and Urban-Rural Development (No. 2020-K-067), Yulin Science and Technology Bureau of Shaanxi Province (No. 2019-101-6), Yulin High-tech Zone Science and Technology Bureau (CXY-2021-10), and Yulin University High-Level Talent Research Start-Up Fund (22GK11).

## Author contributions

YL contributed to writing—original draft preparation, data curation, writing, methodology, and investigation. HZ was involved in writing—original draft preparation, writing—reviewing and editing, and methodology. SC contributed to validation, software, and investigation. HW contributed to writing, conceptualization, and data curation. XL was involved in writing—reviewing and editing, and methodology. WG contributed to investigation and software. All the authors read and approved the final manuscript.

## Authors' information

Yugen Li is a PhD Associate Professor at School of architecture engineering, Yulin University, Yulin 719000, China, and at College of architecture and civil

engineering, Xi'an University of science and technology, Xi'an 710054, China. Huimei Zhang is a PhD Professor at School of Science, Xi'an University of science and technology, Xi'an 710054, China. Shaojie Chen is a PhD Lecturer at College of architecture and civil engineering, Xi'an University of science and technology, Xi'an 710054, China. Hairen Wang is a PhD Lecturer at School of architecture engineering, Yulin University, Yulin 719000, China. Xiaoyu Liu, PhD Lecturer, School of Science, Xi'an University of science and technology, Xi'an 710054, China. Wei Gao, BD Assistant Engineer, Shaanxi Shengyuan Tongtai Construction Engineering Co., Ltd, Yulin 719000, China.

## Funding

This study was supported by National Natural Science Foundation of China (Nos. 52268047, 51868075), Ministry of Housing and Urban-Rural Development (No. 2020-K-067), Yulin Science and Technology Bureau of Shaanxi Province (No. 2019-101-6), Yulin High-tech Zone Science and Technology Bureau (CXY-2021-10), and Yulin University High-Level Talent Research Startup Fund (22GK11).

## Availability of data and materials

All data that support the findings of this study are available from the corresponding author upon reasonable request.

## Declarations

### Competing interests

The authors declare no competing interests.

Received: 15 February 2022 Accepted: 20 December 2022

Published online: 01 March 2023

## References

- ASTM C1585-13, Standard test method for measurement of rate of absorption of water by hydraulic cement concretes, ASTM Committee, 2013.
- Bao, J. W., & Wang, L. C. (2016). Effect of short-term sustained uniaxial loadings on water absorption of concrete. *Journal of Materials in Civil Engineering*, 29(3), 1–12.
- Belleghem, B. V., Montoya, R., Dewanckele, J., Steen, N. V., Graeve, I. D., Deconinck, J., Cnudde, V., Tittelboom, K. V., & Belie, N. D. (2016). Capillary water absorption in cracked and uncracked mortar—a comparison between experimental study and finite element analysis. *Construction and Building Materials*, 110, 154–162. <https://doi.org/10.1016/j.conbuildmat.2016.02.027>
- Bendixen, M., Best, J., Hackney, C., & Iversen, L. L. (2019). Time is running out for sand. *Nature*, 571, 29–31. <https://doi.org/10.1038/d41586-019-02042-4>
- China Academy of Building Research. (2010). *GBT 50082-2009 Standard for test method of long-term performance and durability of ordinary concrete*. Beijing: China Architecture and Building.
- Dong, W., Shen, X. D., Xue, H. J., He, J., & Liu, Y. (2016). Research on the freeze-thaw cycle test and damage model of aeolian sand lightweight aggregate concrete. *Construction and Building Materials*, 123(1), 792–799. <https://doi.org/10.1016/j.conbuildmat.2016.07.052>
- GB, T 50081. (2002). *Standard for test method of mechanical properties on ordinary concrete*. Beijing: China Architecture & Building Pres.
- Gerdas, A., Meier, S., & Wittmann, F. H. (1998). A new application technology for water repellent surface treatment, International conference on water repellent treatment of building materials, Switzerland, Zurich. *Hydrophobe*, 1, 217–230.
- Ghasemzadeh, F., Rashednia, R., Smyl, D., & Pour-Ghaz, M. (2016). A comparison of methods to evaluate mass transport in damaged mortar. *Cement and Concrete Composites*, 70, 119–129. <https://doi.org/10.1016/j.cemconcomp.2016.03.007>
- Gonen, T., Yazicioglu, S., & Demirel, B. (2015). The influence of freezing thawing cycles on the capillary water absorption and porosity of concrete with mineral admixture. *KSCSE Journal of Civil Engineering*, 19(3), 667–671. <https://doi.org/10.1007/s12205-012-0207-7>
- Hall, C. (1989). Water sorptivity of mortars and concrete: a review. *Magazine of Concrete Research*, 41, 51–61. <https://doi.org/10.1680/macrc.1989.41.147.51>

- JGJ 52. (2006). *Standard for technical requirements and test method of sand and crushed stone (or gravel) for ordinary concrete*. Beijing: China Architecture & Building Press.
- Kessler, S., Thiel, C., Grosse, C. U., & Gehlen, C. (2017). Effect of freeze-thaw damage on chloride ingress into concrete. *Materials and Structures*, 50(2), 121. <https://doi.org/10.1617/s11527-016-0984-4>
- Khatib, J. M., & Clay, R. M. (2004). Absorption characteristics of metakaolin concrete. *Cement and Concrete Research*, 34(1), 19–29. [https://doi.org/10.1016/S0008-8846\(03\)00188-1](https://doi.org/10.1016/S0008-8846(03)00188-1)
- Li, G. F., & Shen, X. D. (2019). A Study of the durability of aeolian sand powder concrete under the coupling effects of freeze-thaw and dry-wet conditions. *JOM Journal of the Minerals Metals and Materials Society*, 71(6), 1962–1974. <https://doi.org/10.1007/s11837-019-03440-9>
- Li, Y. G., Zhang, H. M., Liu, G. X., Hu, D. W., & Ma, X. R. (2020). Multi-scale study on mechanical property and strength prediction of aeolian sand concrete. *Construction and Building Materials*, 247, 118538. <https://doi.org/10.1016/j.conbuildmat.2020.118538>
- Li, Y. G., Zhang, M. H., Chen, S. J., Wang, H. R., & Liu, G. X. (2022). Multi-scale study on the durability degradation mechanism of aeolian sand concrete under freeze-thaw conditions. *Construction and Building Materials*, 340, 127433. <https://doi.org/10.1016/j.conbuildmat.2022.127433>
- Liu, L., Qin, G., Zhou, Y., Chen, H. S., & Wang, X. C. (2021). Freezing behavior of unsaturated porous materials. *Construction and Building Materials*, 274, 122112. <https://doi.org/10.1016/j.conbuildmat>
- Liu, L., Shen, D. J., Chen, H. S., Sun, W., Qian, Z. W., Zhao, H. T., & Jiang, J. H. (2014). Analysis of damage development in cement paste due to ice nucleation at different temperatures. *Cement and Concrete Composites*, 53, 1–9. <https://doi.org/10.1016/j.cemconcomp.2014.06.0>
- Lockington, D., Parlange, J. Y., & Dux, P. (1999). Sorptivity and the estimation of water penetration into unsaturated concrete. *Materials and Structures*, 32(5), 342–347. <https://doi.org/10.1007/BF02479625>
- Martys, N. S., & Ferraris, C. F. (1997). Capillary transport in mortars and concrete. *Cement and Concrete Research*, 27(5), 747–760. [https://doi.org/10.1016/S0008-8846\(97\)00052-5](https://doi.org/10.1016/S0008-8846(97)00052-5)
- Parlange, J. Y., Lisle, I. G., Prasad, S. N., & Romkens, M. J. (1984). Wetting front analysis of the nonlinear diffusion equation. *Water Resources Research*, 20(5), 636–638. <https://doi.org/10.1029/wr020i005p00636>
- Tan, Y. Z., Wu, J., Huang, L. B., Wang, H. X., & Zou, Q. J. (2017). The properties evolution process of cement improved soft clay under freeze-thaw cycles effect. *Journal of Building Materials*, 20(2), 373–378. (in Chinese).
- Taniguchi, M., & Katsura, O. (2015). Visualization of the water distribution in the concrete using a humidity sensor. *Concrete Journal*, 53(5), 406–410. <https://doi.org/10.3151/coj.53.406>
- Wang, L. C. (2009). Analytical methods for prediction of water absorption in cement-based material. *China Ocean Engineering*, 23(4), 719–728.
- Wang, Y. R., Cao, Y. B., Zhang, P., Ma, Y. W., Zhao, T. J., Wang, H., & Zhang, Z. H. (2019). Water absorption and chloride diffusivity of concrete under the coupling effect of uniaxial compressive load and freeze–thaw cycles. *Construction and Building Materials*, 209, 566–576.
- Xiao, Q. H., Cao, Z. Y., Guan, X., Li, Q., & Liu, X. L. (2019a). Damage to recycled concrete with different aggregate substitution rates from the coupled action of freeze-thaw cycles and sulfate attack. *Construction and Building Materials*, 221, 74–83. <https://doi.org/10.1016/j.conbuildmat.2019.06.060>
- Xiao, Q. H., Li, Q., Cao, Z. Y., & Tian, W. Y. (2019b). The deterioration law of recycled concrete under the combined effects of freeze-thaw and sulfate attack. *Construction and Building Materials*, 200, 344–355. <https://doi.org/10.1016/j.conbuildmat.2018.12.066>
- Xue, H. J., Shen, X., Liu, Q., Wang, R. Y., & Liu, Z. (2017). Analysis of the damage to aeolian sand concrete surfaces caused by wind-sand erosion. *Journal of Advanced Concrete Technology*, 15(12), 724–737. <https://doi.org/10.3151/jact.15.724>
- Zhang, M. H., Zhu, X. Z., Shi, J. Y., Liu, B. J., He, Z. H., & Liang, C. F. (2022). Utilization of desert sand in the production of sustainable cement-based materials: a critical review. *Construction and Building Materials*, 327, 127014. <https://doi.org/10.1016/j.conbuildmat.2022.127014>
- Zhang, P., Li, D., Qiao, Y., Zhang, S. L., Sun, C. T., & Zhao, T. J. (2018b). The effect of air entrainment on the mechanical properties, chloride migration and microstructure of ordinary concrete and fly ash concrete. *Journal of Materials in Civil Engineering*, 30(10), 04018265.
- Zhang, P., Wittmann, F. H., Lura, P., Mueller, H. S., Han, S., & Zhao, T. (2018a). Application of neutron imaging to investigate fundamental aspects of durability of cement-based materials: a review. *Cement and Concrete Research*, 108, 152–166.
- Zhang, P., Wittmann, F. H., Vogel, M., Müller, H. S., & Zhao, T. J. (2017). Influence of freeze-thaw cycles on capillary absorption and chloride penetration into concrete. *Cement and Concrete Research*, 100, 60–67. <https://doi.org/10.1016/j.cemconres.2017.05.018>
- Zhao, H. T., Ding, J., Huang, Y. Y., Tang, Y. M., Xu, W., & Huang, D. H. (2019). Experimental analysis on the relationship between pore structure and capillary water absorption characteristics of cement-based materials. *Structural Concrete*. <https://doi.org/10.1002/suco.201900184>

## Publisher's Note

Springer Nature remains neutral with regard to jurisdictional claims in published maps and institutional affiliations.

Submit your manuscript to a SpringerOpen® journal and benefit from:

- Convenient online submission
- Rigorous peer review
- Open access: articles freely available online
- High visibility within the field
- Retaining the copyright to your article

Submit your next manuscript at ► [springeropen.com](https://www.springeropen.com)